ACCEPTED ARTICLE PREVIEW

Accepted Article Preview: Published ahead of online publication

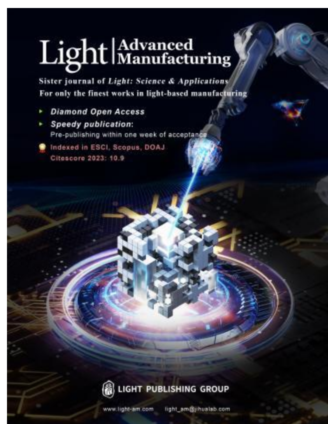

Digital phase-shift mask projection lithography enabling sub-diffraction-limit resolution for dense nanoscale patterning

Yuan-Yuan Zhao, Zi-Xin Liang, Jing-Tao Chen, Wen-Hui Li, Zhi-Cai Wu, Xuan-Ming Duan

Cite this article as: Yuan-Yuan Zhao, Zi-Xin Liang, Jing-Tao Chen, Wen-Hui Li, Zhi-Cai Wu, Xuan-Ming Duan. Digital phase-shift mask projection lithography enabling sub-diffraction-limit resolution for dense nanoscale patterning. *Light: Advanced Manufacturing* accepted article preview 7 May, 2026; doi: 10.37188/lam.2026.080

This is a PDF file of an unedited peer-reviewed manuscript that has been accepted for publication. LAM are providing this early version of the manuscript as a service to our customers. The manuscript will undergo copyediting, typesetting and a proof review before it is published in its final form. Please note that during the production process errors may be discovered which could affect the content, and all legal disclaimers apply.

Received 7 February 2026; Revised 30 April 2026; Accepted 7 May 2026;
Accepted article preview online 7 May 2026

Accepted Manuscript

ACCEPTED ARTICLE PREVIEW

1 # Digital phase-shift mask projection lithography enabling
2 sub-diffraction-limit resolution for dense nanoscale
3 patterning

4 **Yuan-Yuan Zhao[1,2,3,*], Zi-Xin Liang[1,2,3], Jing-Tao Chen[1,2,3], Wen-Hui Li[1,2],**
5 **Zhi-Cai Wu[1,2], and Xuan-Ming Duan[1,2,*]**

6 [1] Guangdong Provincial Key Laboratory of Optical Fiber Sensing and
7 Communications, Institute of Photonics Technology, Jinan University, Guangzhou
8 511443, China
9 [2] College of Physics & Optoelectronic Engineering, Jinan University, Guangzhou
10 510632, China
11 [3] Those authors have equal contributions to this work.

12 * E-mail: yyzhao@jnu.edu.cn and xmduan@jnu.edu.cn

13 ## Abstract

14 The diffraction limit poses a fundamental challenge to digital mask projection
15 lithography (DMPL) in fabricating subwavelength-scale dense periodic patterns,
16 limiting its application in advanced chip manufacturing. To address this, we present a
17 DMPL platform with a resolution-enhancement strategy combining a digital phase-
18 shifting mask with two-photon polymerisation. The method enables precise control of
19 subwavelength structure distribution while preserving DMPL flexibility. Using
20 alternating phase-shifting modulation through cascaded spatial light modulators under
21 517 nm femtosecond laser illumination, we achieve near-physical-limit resolution in a
22 single exposure, producing line patterns with a critical linewidth of ~60 nm
23 (0.16λ/NA) and a single-exposure pitch resolution of ~235 nm (half pitch ~0.32λ/NA).
24 With a double-exposure strategy, the pitch is further reduced to ~158 nm (half pitch
25 ~0.21λ/NA), enabling robust sub-diffraction-limit patterning. This approach advances

Accepted Manuscript

ACCEPTED ARTICLE PREVIEW

26 diffraction-limited patterning and offers new possibilities for manufacturing
27 nanophotonic devices and next-generation microelectronic components.

28 **Keywords:** Digital mask projection lithography, Two-photon polymerisation,
29 Phase-shifting mask, Resolution enhancement, Spatial light modulator, Diffraction
30 limit

31 Introduction

32 With the advancement of conventional photolithography, feature sizes of
33 integrated circuit devices have continuously shrunk from the micrometre scale to the
34 submicrometre and even nanometer scale.[1,2] However, the resolution of
35 photolithography is gradually approaching its theoretical limit.[3,4] Consequently, mask
36 costs, manufacturing complexity, and the demand for extremely high alignment
37 accuracies have increased significantly.[5] Simultaneously, emerging nanophotonic
38 components, such as ultraviolet metalenses and metasurfaces, demand extremely high
39 pattern density, subwavelength feature control, and flexible fabrication capability.[6-9]
40 Maskless projection lithography technology based on spatial light modulators (SLMs)
41 has emerged as a potential solution to address the increasing cost of conventional
42 photolithography.[10-12] It has been extensively investigated as the next-generation
43 lithography technology. For instance, utilising a digital micromirror device (DMD) or
44 a liquid crystal-on-silicon spatial light modulator (LCOS-SLM) to generate digital
45 masks not only reduces the cost of mask fabrication but also enhances lithographic
46 flexibility and production efficiency.[10,13] Although it cannot completely replace the
47 mainstream lithography technology used currently, it simplifies the intricate process
48 of conventional photolithography, thus offering cost-effectiveness, high efficiency,
49 and flexibility. Furthermore, maskless projection lithography can expand the wide-
50 band range of light sources, including continuous, pulsed, and ultrafast femtosecond
51 visible and ultraviolet lasers. [11,12] This indicates its strong technical extensibility and
52 process compatibility, which renders it readily applicable to highly customised
53 photonic and electronic devices. [10,12,13]

Accepted Manuscript

54 To enhance the ultimate resolution of DMD projection lithography, recent efforts
55 typically involve using short wavelengths (193, 248, or 365 nm) coherent light
56 sources,[14-16] incorporating high-density small pixel elements (5.4 μm) in DMD
57 chips,[17-19] and reducing the reduction ratio of the projection lens with a high numerical
58 aperture (NA).[12,20] However, owing to the limited size of individual pixel elements on
59 the DMD chip, which is approximately 10 μm,[17] conventional maskless lithography
60 based on DMD typically adopts a reduction ratio of ~1/5× to ~1/10×, thus resulting in
61 an ultimate resolution at the scale of ~1 μm.[15] As the reduction ratio of the projection
62 lens decreases, for example, to 1/100× – 1/300×,[10] the spacing between adjacent
63 micromirror pixel elements on the DMD chip's focal plane becomes less than 100 nm,
64 which is smaller than the optical diffraction limit (i.e. 0.61λ/NA).[10-12] However, the
65 size of a single pixel element's image cannot exceed the limit, which is approximately
66 200 nm.[10] Consequently, adjacent pixels or multiple elements will inevitably cause
67 image overlap, thereby significantly reducing the lithographic resolution.[18-20]
68 Consequently, neither finer linewidth features nor increased density of fine lines per
69 unit area can be achieved, thereby limiting the information capacity and functionality
70 of individual chips.

71 Phase-shifting mask (PSM) technology is typically employed to enhance the
72 resolution of lithography systems.[21-24] It introduces a π phase difference in adjacent
73 transparent regions, thus creating interference cancellation at the edges of an image to
74 increase contrast and thus improve imaging resolution.[21,24,25] Based on this principle,
75 if PSM technology is applied to maskless projection lithography, it can effectively
76 enhance lithography resolution. However, conventional PSM fabrication requires the
77 deposition of a phase-shifting layer measuring approximately one wavelength and a
78 specific thickness in each designed mask-pattern region.[4,21,24] This is impractical for
79 projection lithography systems without physical mask templates, where depositing a
80 phase-shifting medium layer on programmable digital mask micromirror elements is
81 not feasible.[26]

82 In this study, we propose a method to enhance the resolution of optical projection

Accepted Manuscript

83 lithography using a phase-modulated digital mask, termed digital phase-shifting mask
84 projection lithography (PSM-DPL). Prior to generating digital masks using DMDs or
85 an LCOS-SLM, direct phase modulation of the imaging beam is performed using a
86 pair of cascaded SLMs. This is achieved through pixelated modulation of the
87 illumination light's phase parameters during optical exposure using a computer-
88 controlled SLM. Meanwhile, the interference state between the intensities of adjacent
89 pattern elements on the image plane is altered by introducing a phase difference (or
90 odd multiples) in the adjacent micromirror pixel areas. This causes interference
91 cancellation in the projection of adjacent elements, thus reducing the intensity of dark
92 areas in the light-field distribution and enhancing the intensity of bright areas.
93 Consequently, the imaging contrast and resolution of projection lithography are
94 improved.

95 Systems and Principles

96 PSM-DPL system and resolution-enhancement principle

97 The PSM-DPL system is illustrated in Figure 1a. The light source is a femtosecond
98 pulse laser with a central wavelength of 517 nm, a repetition rate of 10 MHz, and a
99 pulse width of ~240 fs. The collimated and uniformised flat-top optical field is
100 modulated by the digital mask, thus resulting in pixel-controlled patterned optical-
101 field information with independent amplitudes and phases. Subsequently, this
102 patterned target optical field is projected onto the photoresist and rendered smaller
103 using the projection lens system, which includes a tube lens (f = 200 mm), an NA of
104 1.40, and a 100× oil-immersion objective lens, thereby achieving precise exposure of
105 the target pattern. Additionally, the system includes a real-time monitoring unit to
106 ensure the correct transmission of optical-field information during the exposure
107 process. A detailed description of the PSM-DPL system is provided in Supplementary
108 Figure S1.

109 The programmable digital mask can generate arbitrary target patterns, with dense
110 line patterns as an example. When the designed line-to-line spacing is excessively

Accepted Manuscript

ACCEPTED ARTICLE PREVIEW

111 small, the optical fields of adjacent lines overlap at the focal plane of the objective
112 lens and become indistinguishable, as shown in the inset of Figure 1a. However, the
113 programmable PSM introduces a phase difference of π between adjacent patterns, thus
114 altering the interference overlap status of the original adjacent patterns.[27] This
115 changes them from an interference phase overlap to an interference phase cancellation,
116 thereby creating a zero-field region in the middle of adjacent line patterns.
117 Consequently, the brightness and darkness of the optical field change significantly,
118 thus enhancing the contrast of the patterns and improving the resolution under
119 identical exposure conditions.

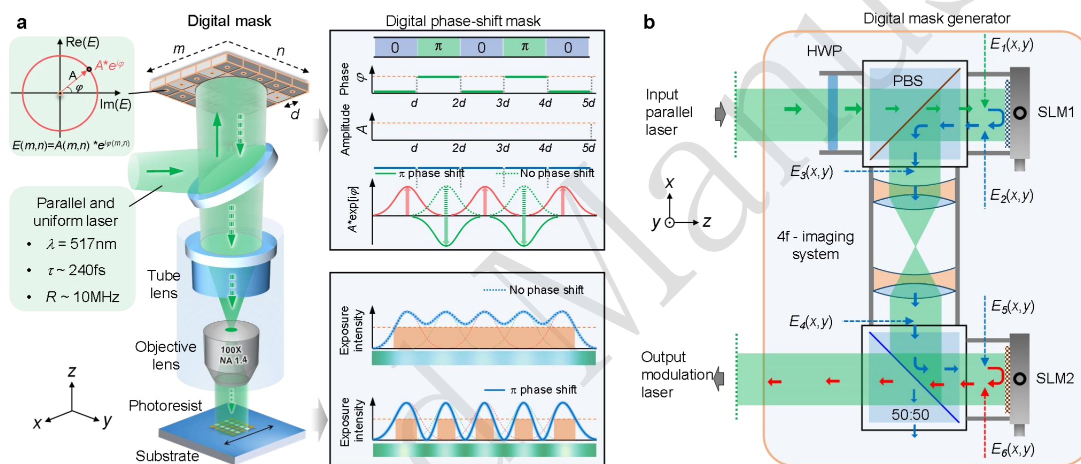

120

121 **Figure 1. Scheme of the experimental system and method for digital phase-shift mask**
122 **projection lithography. a,** A Typical digital mask projection lithography system, including the
123 light source, digital mask, projection optical components (tube lens and objective lens),
124 photoresist, and substrate. The digital mask shown in the upper inset generates amplitude- and
125 phase-modulated patterned light fields, such as dense wire grid patterns. The inset below shows a
126 comparison of exposure results with and without a PSM. The adjacent line patterns, which
127 introduce π phase shifts, have resolvable spacing and higher pitch resolution. **b,** Optical path
128 subsystem of digital mask generates a patterned PSM through amplitude- and phase-type LCOS-
129 SLM cascade modulation of light field. SLM1 and SLM2 are amplitude- and phase-type SLMs,
130 respectively.

131 ## Digital phase-shift mask generation method and system

132 The amplitude and phase information of the target pattern are independently
133 modulated with high flexibility through a cascaded configuration of amplitude- and
134 phase-type LCOS-SLMs, as shown in Figure 1b. Collimated and linearly polarised

Accepted Manuscript

ACCEPTED ARTICLE PREVIEW

135 light passes through a half-wave plate and a polarisation beam splitter before entering
136 the amplitude-type LCOS-SLM, where it undergoes amplitude modulation. The half-
137 wave plate's angle is adjusted to ensure maximum utilisation of the incident light. The
138 polarisation beam splitter serves as an input/output polariser and, in conjunction with
139 the amplitude-type LCOS-SLM, modulates the polarisation state of the reflected light,
140 thereby changing the output intensity. This results in amplitude modulation.
141 Subsequently, the optical field containing the amplitude information of the target
142 pattern is directed into a 4F pixel-matching system comprising two identical tube
143 lenses with a 1:1 magnification ratio and is then incident on the phase-type LCOS-
144 SLM (Figure 1b). This system accomplishes the composite modulation of the optical-
145 field information, including both amplitude and phase. The amplitude- and phase-type
146 LCOS-SLMs have the same parameters, such as image plane size, resolution (1080 ×
147 1920 pixels), and pixel size (8 μm × 8 μm) (see Table S1). The 1:1 pixel-matching
148 system (Figures S2 and 2a), which serves as a relay between the amplitude- and
149 phase-type LCOS-SLMs, corrects aberrations during propagation,[28] thus ensuring
150 perfect alignment of single-pixel amplitude information with pixel information. Using
151 the programmability of digital masks, different greyscale values can be independently
152 loaded onto any pixel as required, thus enabling high degrees of spatial light-field
153 control (Figures S3 and S4).

154 By independently controlling the amplitude and phase of the optical field using
155 two LCOS-SLMs and cascading the two modulators using a 4F system (Figures 1b
156 and 2a), the complex amplitude of the optical field is obtained as the output.
157 Horizontally polarised light incident on the amplitude-type LCOS-SLM can be
158 represented by the Jones matrix as follows:

$$E_1(x, y) = A_0(x, y) \begin{bmatrix} 1 \\ 0 \end{bmatrix} \tag{1}$$

159 where, x and y denote the pixel coordinates, and $A_0(x,y)$ represents the optical field's
160 amplitude corresponding to x and y. The LCOS-SLM alters the polarisation direction
161 of the optical field, and we define the rotation matrix as follows:

Accepted Manuscript

$$M_{slm} = \begin{bmatrix} \cos\theta & \sin\theta \\ -\sin\theta & \cos\theta \end{bmatrix} \tag{2}$$

The output optical field after amplitude modulation is

$$E_2(x,y) = M_{slm}E_1(x,y) = A_0(x,y)\begin{bmatrix} \cos\theta \\ -\sin\theta \end{bmatrix} \tag{3}$$

The optical field is reflected by a PBS prism, and the PBS prism reflects only vertically polarised light.

$$E_3(x,y) = \begin{bmatrix} 0 & 0 \\ 0 & 1 \end{bmatrix} E_2(x,y) = A_0(x,y)\begin{bmatrix} 0 \\ -\sin\theta \end{bmatrix} \tag{4}$$

The optical field is directed through a 50:50 beam splitter prism and enters the phase-type LCOS-SLM, which modifies the optical path difference in the liquid crystal to alter the phase. The output optical field after phase modulation is

$$E_4(x,y) = e^{j\varphi(x,y)}E_3(x,y) = A_0(x,y)e^{j\varphi(x,y)}\begin{bmatrix} 0 \\ -\sin\theta \end{bmatrix} \tag{5}$$

The optical field after composite modulation is denoted as $E_4(x,y)$.

Figure 2. Light-field amplitude, phase pixelation modulation of digital mask, and pixel-size matching, alignment, and detection. a, Optical system of pixel-size matching and alignment. (focal lengths: f_1 = 100 mm, f_2 = 100 mm). **b,** Measured light-field intensity of digital mask produced via single amplitude-type SLM1 and phase-type SLM2. Amplitude mask (SLM1) is arranged as -1-1-0-(2 pixels (1):1 pixel (0)). Phase mask (SLM2) is arranged as a group of 3 pixels, with alternating 0 and π. **c,** Measured two-dimensional (2D) light-field intensity distribution of composite mask (SLM1+SLM2). Spatial arrangements of amplitude $A(x,y)$ and phase $\varphi(x,y)$ are -1-1-0-1-1-0- and -0-0-0-π-π-π-, respectively. **d,** Measured 2D light-field intensity distribution of

Accepted Manuscript

ACCEPTED ARTICLE PREVIEW

composite mask (SLM1+SLM2). Spatial arrangements of amplitude $A(x,y)$ and phase $\varphi(x,y)$ are -1-1-0-1-1-0- and -0-π-π-π-0-0-, respectively. Pixels in phase are shifted by one unit, as compared with Figure (c).

Compared with other composite modulation systems (see Table S2 and Figure S5), this system enables independent, single-pixel-level control of the optical field with high flexibility. [29-31] This system enables both the amplitude and phase of the optical field to be controlled independently while fully utilising the resolution of the SLM target surface. In theory, provided that the individual pixels of the modulator are sufficiently small and the number of pixels with a wide range of grey levels is sufficient, this system can generate digital-mask patterns of any arbitrary topological shape. This capability enables the replacement of conventional photolithography photomasks entirely, thereby offering high flexibility and cost-effectiveness for digital PSM-DPL.

Results

Amplitude and phase modulation of the projected light field

The precise control of digital phase-shift masks imposes single-pixel-level alignment requirements for loading patterns onto both amplitude- and phase-type LCOS-SLMs. Figure 2a illustrates the optical path diagram of the 4F image system, which ensures the matching and alignment of the pixel sizes of the two SLMs. The positions of pixels in the amplitude- and phase-type LCOS-SLMs are centrally symmetric and flipped both vertically and horizontally. Considering a 3 3-pixel-pitch line pattern as an example, we captured the optical-field distribution images for pure amplitude modulation and pure phase modulation using an optical spot quality analyser (Femto Easy Beam Pro), as shown in Figure 2b. The amplitude-type LCOS-SLM loaded a 2-pixel (255):1-pixel (0) periodic line pattern, whereas the phase-type LCOS-SLM only performed reflections, thus resulting in a wave trough of optical intensity at a pixel value of 0. In the case of pure amplitude modulation, the wave peak of optical intensity was located at the centre of two bright pixels (255), which

Accepted Manuscript

ACCEPTED ARTICLE PREVIEW

206 decrease on both sides, thus reflecting a Gaussian distribution. For pure phase
207 modulation, a 3-pixel (π):3-pixel (0) periodic line pattern was used. In this case, the
208 optical field exhibited troughs at the 0 and π phase transitions (Refer to Figure S6).
209 Both optical-field distributions exhibit periodicity with a pitch of 24 μm (3 pixels).

210 The pixels of the two SLMs were aligned using a six-axis optical adjustment
211 mount, as shown in Figure S2. By loading the corresponding patterns onto the
212 amplitude- and phase-type LCOS-SLMs, the position of the phase-modulation
213 optical-intensity trough aligned with the position of the pure amplitude optical-
214 intensity trough, thus achieving a programmable 'digital phase shift mask'. At this
215 point, the phase-shift pattern loaded onto the phase-type LCOS-SLM—featuring 0
216 and π phase transitions—aligns precisely between the two bright patterns of the
217 amplitude-type LCOS-SLM. The captured optical field exhibits a periodic
218 characteristic with a 24 μm (3-pixel) interval, similar to the single amplitude
219 modulation optical field (Figure 2b top), as shown in Figure 2c. Simultaneously, using
220 the six-axis optical adjustment mount (AMM6-1A, LBTEK) for the precise
221 translation of one pixel (8 μm), the 0 and π phase transitions of the phase-type LCOS-
222 SLM are shifted to the exact centre of the bright pixel (1) in the amplitude pattern.
223 This splits the original two-pixel peak into two single peaks. Compared with the
224 alignment presented in Figure 2c, the number of peaks in the optical field doubled, as
225 shown in Figure 2d. At this point, one may conclude that a one-pixel alignment
226 deviation exists between the two LCOS-SLM pixels relative to the target PSM
227 configuration (see Figure S7).

228 **Resolution limit of amplitude- and phase-only modulation DPL**

229 To demonstrate the advantages of phase-shift masks over conventional amplitude
230 masks in projection lithography, we first investigated the lithographic limits of
231 periodic line patterns with either pure amplitude or phase modulation. When using the
232 amplitude-type LCOS-SLM to load different patterns, the phase-type LCOS-SLM
233 loaded patterns with a greyscale value of 0. In this default configuration, the system

Accepted Manuscript

ACCEPTED ARTICLE PREVIEW

234 does not apply phase modulation to the optical field; this is referred to as pure
235 amplitude modulation. Conversely, when using the phase-type LCOS-SLM to load
236 different patterns, the amplitude-type LCOS-SLM loaded patterns with a greyscale
237 value of 255. In this case, the system does not apply amplitude modulation to the
238 optical field and uniformly outputs the maximum amplitude; this is referred to as pure
239 phase modulation. Figure 3a shows the exposure results for pure amplitude
240 modulation when the amplitude-type LCOS-SLM loaded 2-pixel-wide lines with line
241 spacings ranging from 1 to 8 pixels, which corresponds to periods from 3 to 10 pixels.
242 Under experimental conditions with an incident laser power of 2.84 mW and an
243 exposure time of 40 s, for 2-pixel-wide digital mask line patterns, the photoresist line
244 widths ranged from 144 to 159 nm, while the experimental period widths varied from
245 391 to 768 nm. When the line period reduced to less than 4 pixels, the line arrays
246 merged and became indistinguishable.

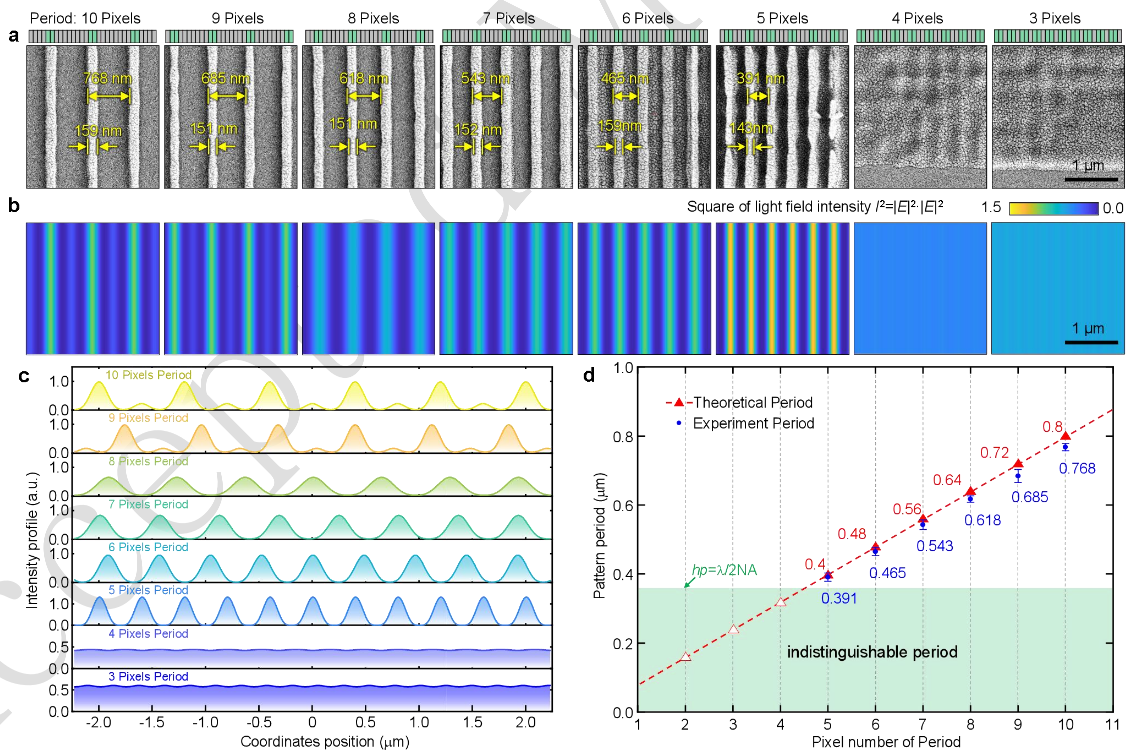

247

248 **Figure 3. Exposure results of different periodic line patterns under pure amplitude**
249 **modulation. a,** Scanning electron microscopy images of photoresist patterns exposed by pure
250 amplitude digital masks with different periodic line patterns ranging from 10 to 3 pixels. **b,**
251 Theoretically calculated 2D optical-field distribution for different periodic line patterns. **c,**

Accepted Manuscript

ACCEPTED ARTICLE PREVIEW

252 Theoretically calculated intensity profiles for different periodic line patterns. **d,** Comparison of
253 theoretical and experimental periodic widths for 2-pixel wide lines with pure amplitude
254 modulation at different pixel periods. Periods smaller than 5 pixels are defined as forbidden
255 periods.

256 We computed the focal-plane optical-field distributions for lines with different
257 periods while considering the two-photon nonlinear absorption effect.[11,12] We plotted
258 the square of the optical intensity distribution (see Supplementary Note 5 for the
259 detailed calculation method), as shown in Figure 3b. Theoretical calculations indicate
260 that, in the absence of a phase-shift mask, the minimum pattern period that can be
261 exposed was 400 nm (~1.1λ/NA), corresponding to a 5-pixel period line pattern mask.
262 This conclusion represents 'the general sparrow criterion' for parallel projection
263 lithography (see Supplementary Note 6 and Figure S8).[12,32,33] As the line period
264 continued to decrease, the optical fields overlapped and became indistinguishable (see
265 Figure 3c). The theoretically and experimentally obtained line periods increased
266 linearly with the number of pixels, which were slightly smaller than the theoretical
267 period (Figure 3d). This discrepancy arises from the scaling-factor correction of the
268 projection imaging system, i.e. 1/102 × (Figure S9), which is consistent with
269 theoretical predictions. When the line period decreased to 4 pixels and below, the
270 half-pitch of the lines (*hp*) became smaller than 0.5λ/NA, thus appearing in the
271 forbidden period.[33-36] Consequently, the digital mask cannot be sharply imaged in the
272 photoresist through the projection lens, which implies that the lines cannot be exposed
273 effectively.

274 In this projection optical system, the resolution limit of the line pitch for pure
275 amplitude modulation is 400 nm (~1.1 λ /NA).[12,36] Amplitude-only modulation can
276 yield complex topological patterns within the ultimate resolution. By contrast, the
277 resolution limit of the line pitch for phase-only modulation is 240 nm (~0.67λ/NA), as
278 shown in Figures S10 and S11, which corresponds to the phase LCOS-SLM loaded
279 with a half-pitch 3-pixel pattern. However, phase-only modulation cannot generate
280 complex topological patterns independently, and the achieved structural width is
281 larger. The PSM modulation technique complements the advantages of both

Accepted Manuscript

ACCEPTED ARTICLE PREVIEW

282 techniques by achieving a smaller resolution while maintaining the independence and
283 integrity of the patterns. Considering the example of loading a 2-pixel wide line with
284 a 3-pixel pitch using amplitude modulation, the phase-type SLM must load a 3-pixel
285 pitch line pattern with phases 0 and π arranged alternately to achieve a phase
286 difference $\Delta\varphi$ of π between adjacent lines, as shown in the top inset of Figures 4a–c.
287 The loaded patterns of the phase-type SLM are half the period of the loaded pattern of
288 the amplitude-type SLM. This arrangement ensures that adjacent periods of the
289 amplitude pattern have a phase difference of π.

290 **Resolution limit of PSM modulation DMPL**

291 For the digital mask with a 2-pixel width and 3-pixel pitch, the exposed resist
292 patterns by amplitude-only modulation are indistinguishable, as shown in Figure 4a,
293 whereas both phase-only and PSM modulations can generate clear and dense line
294 pattern structures, with simulated periods of 238 nm, as shown in Figure 4d. Based on
295 the experimental results, both methods exhibited a period width of 235 nm, which
296 closely matched the simulation results. However, the linewidths were 214 and 146 nm,
297 respectively, with the alternating PSM technique achieving a narrower linewidth. By
298 adjusting the exposure dose, the CD:gap of the line array pattern was controlled to 1:1
299 or smaller (Figures S12 and S13). By combining the simulated and experimental
300 results, we obtained the widths of structures with a 2-pixel width and different pixel
301 periods (see Figure 4e). For periods greater than 5 pixels (including 5 pixels),
302 amplitude-only modulation can expose dense line patterns. For periods of 3 and 4
303 pixels, the PSM modulation must achieve clear exposure. For structures with periods
304 smaller than 3 pixels (excluding 3 pixels), because the diffraction limit of this system
305 is 217.5 nm (0.5λ/NA), none of the methods—pure amplitude modulation, pure phase
306 modulation, or alternating PSM—can produce structures beyond this resolution.

Accepted Manuscript

ACCEPTED ARTICLE PREVIEW

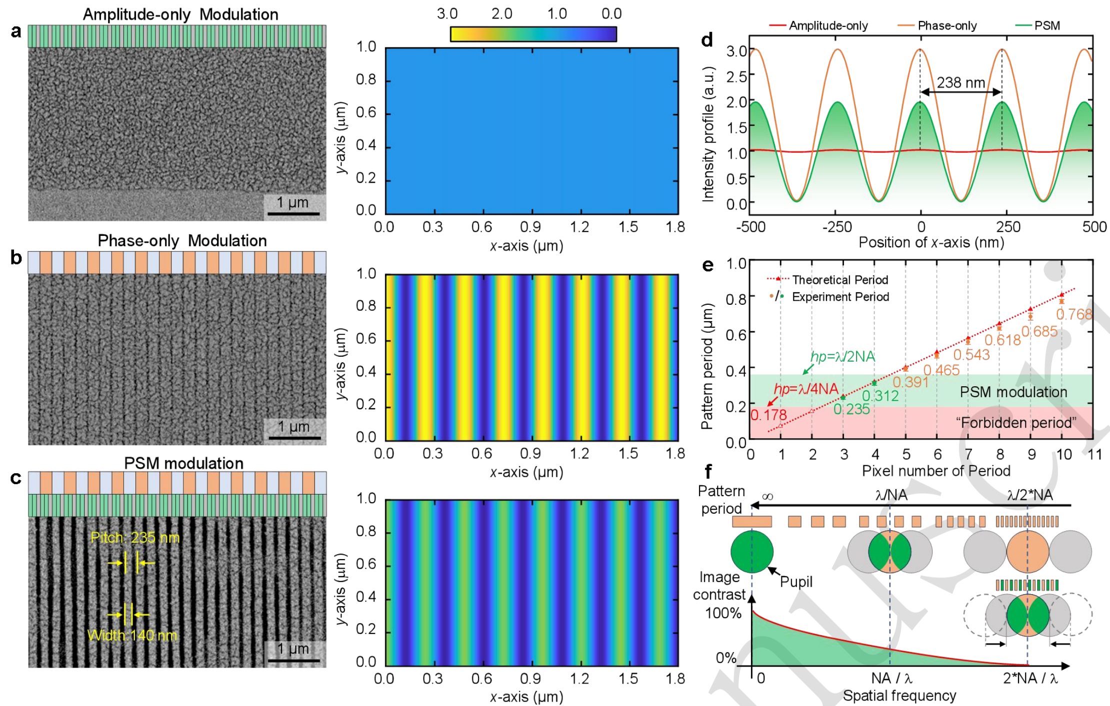

307

308 **Figure 4. Comparative analysis of exposure results for periodic line-space patterns**
309 **generated using digital mask strategies. a,** SEM images and simulated optical-field distribution
310 of periodic lines (2 pixels (255):1 pixel (0)) under amplitude-only modulation. **b,** SEM images and
311 simulated optical-field distribution of periodic lines (3 pixels (0):3 pixels (π)) under phase-only
312 modulation. **c,** SEM images, and simulated optical-field distribution of periodic lines under PSM
313 modulation. **d,** Comparison of light-intensity profiles for periodic line-space patterns generated
314 using different digital mask strategies. **e,** Relationship between pattern period and pixel count for
315 three types of digital masks. **f,** Modulation transfer function (MTF): contrast loss is proportional to
316 the zero-order light passing through the lens aperture without an interference partner, which only
317 contributes to a constant offset.

318 According to the principles of information optics, when light passes through an
319 object and undergoes diffraction, the high-frequency components in the diffraction
320 spectrum contain more detailed information about the object.[36,37] For digital masks in
321 the form of periodic gratings, the distribution of their diffraction spectrum is centered
322 around the zeroth-order diffraction spectrum and is symmetrical.[38-40] In a projection
323 lithography system, owing to the low-pass filtering effect in the objective system,
324 only a portion of the diffraction spectrum of the digital mask can be received by the
325 objective and interfere to form an image on the image plane.

326 In the case of on-axis point-source illumination,[40-42] when the period of the
327 grating-type mask pattern is such that its first-order diffraction light coincides with the

Accepted Manuscript

ACCEPTED ARTICLE PREVIEW

328 aperture edge of the projection objective, the half pitch of this striped pattern is the
329 maximum resolution that the lithographic system can resolve,[41] as shown in Figures
330 4f and S14. When the half pitch of the striped pattern is smaller than this value, the
331 first-order diffraction light appears outside the aperture of the projection objective,
332 and only the zeroth-order light passes through the projection objective, thus rendering
333 interference imaging on the image plane impossible. Under on-axis point source
334 illumination, the cutoff frequency of the projection system is NA/λ.[32,33,40-42] This
335 implies that the theoretical resolution limit of a conventional projection lithography
336 imaging system is R = hp (pitch/2) = λ/(2NA), which corresponds to a theoretical
337 period of pitch = λ/NA = 356 nm. For digital phase-shift mask projection lithography,
338 the theoretical resolution limit is R = hp (pitch/2) = λ/4NA, which corresponds to a
339 theoretical period of pitch = λ/(2NA) = 178 nm, as shown in Figures 4c and S15. The
340 alternating phase-shift mask technique creates phase conflicts between adjacent
341 structures and utilises the dark regions of optical intensity generated by interference
342 cancellation to render the originally indistinguishable structures clear and resolvable.

343 **Optimal phase-shift value of the digital mask**

344 To investigate the relationship between phase shift Δφ and optical-field
345 distribution in alternating PSM technology, we selected grey levels of 64, 128, 192,
346 and 255, which correspond to phase delays Δφ of 0.17π, 0.40π, 0.75π, and 1.05π,
347 respectively. A 2-pixel-wide, 4-pixel-pitch array structure was used, with the
348 minimum grey level in the graphics loaded onto the phase-type LCOS-SLM set to 0.
349 The effects of alternating PSM modulation at different maximum phase delays Δφ
350 were compared, as shown in Figures 5a and 5b. As Δφ approached π, the peak
351 intensity, contrast, and slope between light and dark regions increased continuously
352 and reached maximum values when Δφ ≈ π. By contrast, pure amplitude modulation
353 and low phase delays (e.g. 0.17π) only marginally resolved the photoresist structures
354 due to low local contrast in the optical field (Figure 5c). Furthermore, as Δφ
355 approached π, the number of peaks in the intensity distribution doubled, thus
356 indicating that the highest spatial contrast can be achieved using this configuration.

Accepted Manuscript

ACCEPTED ARTICLE PREVIEW

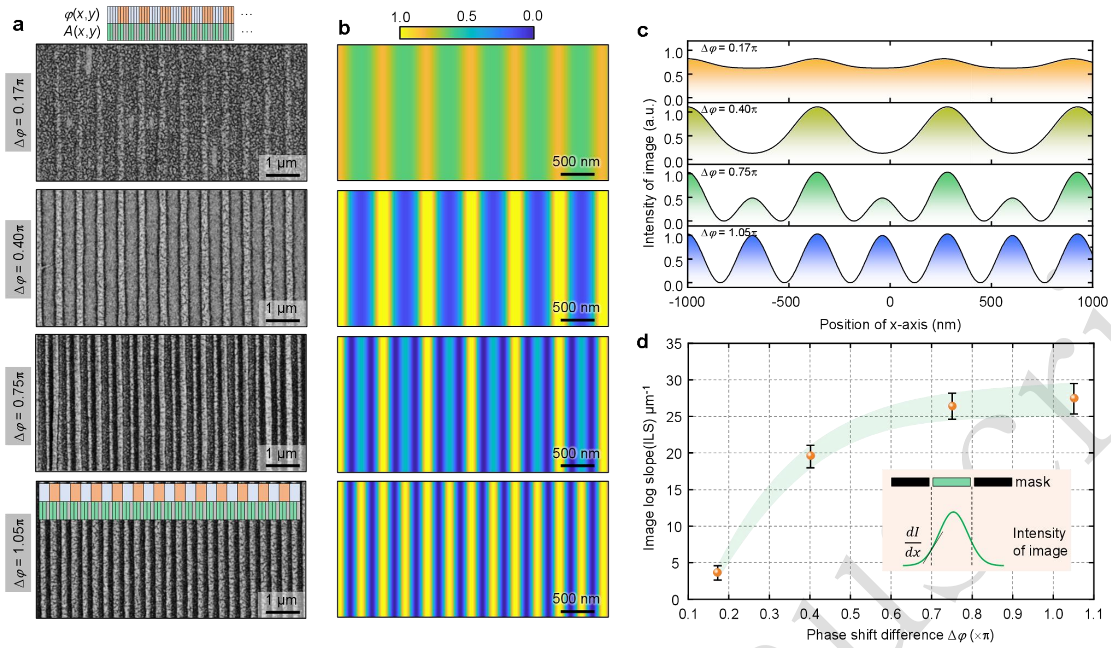

357

358 **Figure 5. Comparative analysis of exposure results for extreme periodic lines under phase-**
359 **shift mask modulation with different phase shifts $\Delta\varphi$. a,** SEM images and simulated optical-
360 field distribution of periodic lines under PSM modulation with different phase shift $\Delta\varphi$ ranges
361 from 0.17π to 1.05π. **b,** Simulated optical-field distribution of periodic lines under PSM
362 modulation with different phase shift $\Delta\varphi$ ranges from 0.17π to 1.05π. **c,** Light-intensity profile for
363 periodic line-space patterns with different phase shifts. **d,** Relationship between ILS and phase-
364 shift difference $\Delta\varphi$. Inset illustrates slope of optical-field intensity.

365 In photolithography, when controlling the line width of the photoresist pattern
366 exerts a greater effect on lithographic performance, the key metric that affects the
367 lithographic results is the image log slope (ILS) at the ideal linewidth edge.[43-45] The
368 ILS quantifies the steepness of the intensity transition at feature boundaries and is
369 expressed as

$$ILS = \frac{1}{I} \cdot \frac{dI}{dx} = \frac{d\text{In}(I)}{dx} \quad (6)$$

370 Typically, the ILS is evaluated at the mask-pattern boundary (see inset of Figure 5c).
371 For structures with pitches of 3–4 pixels, pure amplitude modulation alone caused a
372 rapid decrease in the optical-field contrast after passing through a 1/100× objective,
373 thus rendering it difficult to clearly resolve bright and dark stripes.

374 In this study, the ILS is used as a quantitative metric to guide the optimisation of
375 Δφ in phase-modulated exposures. A higher ILS corresponds to a steeper intensity

Accepted Manuscript

ACCEPTED ARTICLE PREVIEW

376 gradient, which enhances the pattern contrast and reduces the linewidth. As $\Delta\varphi$
377 approaches π, destructive interference between adjacent pixels suppresses sidelobes
378 and creates more pronounced intensity minima, thus resulting in sharper feature edges
379 and higher ILS values. Therefore, the optimal $\Delta\varphi$ is determined by maximising the
380 ILS, thereby effectively improving both imaging contrast and resolution.

381 **Lithography verification of metal-layer patterns in chip layout**

382 This study demonstrates a digital projection lithography approach based on PSM
383 modulation, which achieved a pitch resolution of 235 nm with a single exposure, i.e. a
384 value close to the physical resolution limit of digital lithography.[4,12,36] We validated
385 the feasibility of using PSM digital lithography for integrated circuit patterning by
386 fabricating two representative metal-layer layouts (Figures 6a and 6b) and a grating
387 map (Figure S16). For the dense regions of the ordered layout shown in Figures 6a,
388 S17a, and S18, PSM lithography enabled the effective exposure of features that were
389 otherwise unresolvable. Even in the unordered layout presented in Figures 6b and
390 S17b, the method successfully generated numerous dense lines with an interline pitch
391 of 276 nm, which is below the diffraction limit of λ/NA.

392 Compared with the case of conventional photolithography, as shown in Figure 6c,
393 the achieved resolutions correspond to the 130 and 90 nm technology nodes (green
394 area), thus highlighting the potential of this method as a viable alternative for chip
395 patterning at the 90 nm node.[46-50] Combining the method with the multiple exposure
396 process,[12,36] the pitch can reach 158 nm with double exposure (Figure S19). If the
397 method is further replaced with 400 nm laser exposure, then a 28 nm lithography
398 process node (blue area) can be expected.

Accepted Manuscript

399 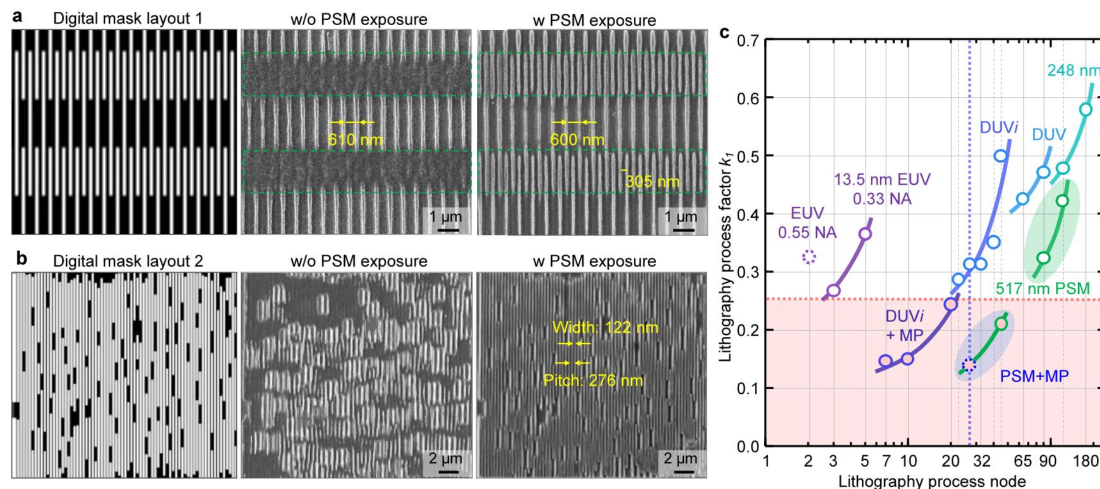

400 **Figure 6. Performance (pitch resolution) comparison for chip metal-layer layout. a,** Digital
401 mask and SEM images of ordered layout. **b,** Digital mask and SEM images of unordered layout. **c,**
402 Statistical results of pitch-resolution and process factor of DMPL compared with 248 and 193 nm
403 deep-ultraviolet (DUV) and extreme ultraviolet (EUV) lithography.

404 Unlike conventional lithography, the proposed digital PSM lithography technique
405 is maskless, inexpensive, highly flexible, and customisable. These features
406 significantly simplify the fabrication process, reduce the time from chip design to
407 prototyping, and reduce research and development costs.[15,26] This technology provides
408 a novel solution for multi-variety, small-batch, and customised chip fabrication, and
409 establishes a promising foundation for future high-precision manufacturing at sub-
410 100 nm scales.

411 Additionally, the arbitrary and independent control of both amplitude and phase
412 provided by the dual-SLM platform renders this DMPL approach particularly suitable
413 for fabricating complex, nonperiodic micro–nano optical components, such as
414 metasurfaces and diffractive optical elements. Future studies will focus on system
415 optimisation and process refinement to further improve pattern fidelity and fabrication
416 stability. Additionally, integration with other advanced manufacturing techniques,
417 such as multiphoton polymerisation and deep ultraviolet lithography, will also be
418 explored to broaden the applicability of this approach to broader nanofabrication
419 scenarios.

420

Accepted Manuscript

ACCEPTED ARTICLE PREVIEW

421 ## Discussion

422 In this study, we developed PSM-DPL technology by combining the flexibility of
423 SLMs with the resolution-enhancing advantages of conventional PSM techniques,
424 thereby enabling the efficient fabrication of subwavelength-scale dense line patterns.
425 Experimental results demonstrate that this technology can achieve line patterns with a
426 feature width of ~60 nm (CD ~0.16λ/NA) and a pitch resolution of ~235 nm (*hp*
427 ~0.32λ/NA) in a single exposure, thus approaching the physical resolution limit of
428 digital lithography. Through double exposure, the achievable pitch resolution was
429 further improved from 235 to 158 nm, thereby validating the feasibility of this method
430 for patterning metal layers of integrated circuits. By precisely controlling the phase
431 difference ($\Delta\varphi = \pi$) between adjacent patterns and leveraging destructive interference
432 effects, imaging contrast and resolution are enhanced. Both experimental and
433 simulation results confirm that when the phase difference approaches π, the contrast
434 of the optical-field distribution and the ILS reach their optimal values, thus achieving
435 resolution near the diffraction limit.

436 Compared with conventional lithography techniques, digital PSM lithography
437 offers several distinct advantages. First, its maskless nature eliminates the necessity
438 for expensive physical mask fabrication, thereby substantially reducing both
439 development time and expenses. Second, the use of a programmable SLM enables
440 high patterning flexibility, thus allowing the rapid generation of arbitrarily complex
441 designs and rendering the approach particularly suitable for multi-variety, small-batch,
442 and customised chip fabrication. Third, the technique is compatible with a wide range
443 of illumination sources spanning from visible to ultraviolet wavelengths, thereby
444 facilitating seamless integration with other advanced manufacturing platforms,
445 including multiphoton polymerisation and deep ultraviolet lithography. Collectively,
446 these advantages highlight the strong potential of digital PSM lithography as a
447 versatile and cost-effective strategy for fabricating subwavelength-scale line patterns.
448 Beyond providing a promising alternative to conventional lithographic methods, this

Accepted Manuscript

449 approach can facilitate high-density integrated circuit manufacturing and the
450 development of broader micro- and nanofabrication applications.

451 Materials and Methods

452 Experimental setup

453 We used a complex amplitude-modulation digital-mask projection lithography
454 system equipped with an ultrafast fibre femtosecond laser system (Huaray Precision
455 Laser Co., Ltd.), which delivered a repetition rate of f = 10 MHz, a central
456 wavelength of 517 nm, and a pulse duration of 240 fs, as shown in Figure S1. After
457 the outgoing laser beam was expanded and homogenised, it entered the complex
458 amplitude-modulation system. Some of the energy of the complex amplitude-
459 modulation light field entered the charge-coupled device (CCD) to achieve real-time
460 observation of the light field during lithography. The main light energy entered the
461 oil-immersed objective lens (100×, NA 1.40, Nikon) to transfer the scaled image to
462 the photoresist surface. In this system, tube lens1 and lens2 were exactly the same
463 tube lenses (TTL100-A, Thorlabs). Unlike ordinary lenses, the main imaging system
464 used tube lenses to reduce imaging aberrations. The photoresist substrate was placed
465 on an electrically controlled translation stage. The translation stage can be a three-
466 dimensional translation stage (AG10010H, OptoSigma) with an *XY*-plane
467 displacement accuracy of 1 μm and a high *Z*-axis displacement accuracy of 0.1 μm.
468 Combined with real-time CCD observations, the optimal focal position of the
469 lithography process can be guaranteed.

470 Sample fabrication

471 AR-N 7520 (Allresist GmbH) was used as the photoresist in the experiment. The
472 photoresist film was prepared via spin coating at 5000 rpm for 1 min using a spin
473 coater (MIDAS SYSTEM SPIN-1200T) on a glass substrate, thus resulting in a
474 photoresist thickness of 260 nm. Subsequently, the coated substrate was prebaked on
475 a hot plate at 85°C for 1 min. After photoresist exposure, post-bake was not required.

Accepted Manuscript

ACCEPTED ARTICLE PREVIEW

476 Instead, the substrate was directly immersed in an AR300-47 developer solution
477 (Allresist GmbH) for 90 s. Subsequently, the residual developer solution on the glass
478 substrate was rinsed with deionised water, and the surface was dried by blowing
479 nitrogen gas. This process resulted in the formation of a photoresist pattern on the
480 substrate.

481 **Sample characterisation**

482 Surface and feature-scale analyses of line-array patterns were performed using a
483 field-emission scanning electron microscope (Thermo Scientific FEI, Apreo 2 SEM).
484 The thickness of the photoresist film was measured using a probe surface
485 profilometer (KLA-Tencor Corp., AlphaStep P-7).

486 **Acknowledgments**

487 This study was supported by the National Key Research and Development Program
488 of China (2016YFA0200500), the National Natural Science Foundation of China
489 (62575128), the Major Talent Program of Guangdong Province (2019CX01Z389),
490 the Science and Technology Planning Project of Guangzhou (202007010002), and
491 the Guangdong Basic and Applied Basic Research Foundation (2023A1515011404).

492 **Author Contributions**

493 X.-M.D. supervised the project. Y.-Y.Z and X.-M.D. conceived the experiments. Y.-
494 Y.Z, Z.-X.L, and Z.-C.W. constructed the experimental setup. W.-H.L, J.-T. C, and
495 Z.-C.W. performed the experiments. Z.-X.L and J.-T. C. developed numerical
496 methods to simulate the optical fields. Y.-Y.Z wrote the manuscript. All authors
497 participated in data analysis and contributed to the writing of the manuscript.

498 **Data availability**

499 The data supporting the findings of this study are available from the corresponding
500 author upon request.

501 **Conflict of interest**

Accepted Manuscript

ACCEPTED ARTICLE PREVIEW

502 The authors declare no competing interests.

503 **Supplementary information**

504 Supplementary materials are available in the online version.

505 ## References

506 1. Wagner, C. & Harned, N. Lithography gets extreme. *Nature Photonics* **4**,
507 24-26 (2010).
508 2. Sharma, E. et al. Evolution in lithography techniques: microlithography
509 to nanolithography. *Nanomaterials* **12**, 2754 (2022).
510 3. Ito, T. & Okazaki, S. Pushing the limits of lithography. *Nature* **406**, 1027-
511 1031 (2000).
512 4. Erdmann, A. Optical and EUV Lithography: A Modeling Perspective
513 (Bellingham: SPIE, 2021).
514 5. Zhang, J. C. et al. Non-local bound states in the continuum for
515 nanoscale alignment. *Nature Photonics* **20**, 296-300 (2026).
516 6. Tseng, M. L. et al. Vacuum ultraviolet nonlinear metalens. *Science*
517 *Advances* **8**, eabn5644 (2022).
518 7. Semmlinger, M. et al. Generating third harmonic vacuum ultraviolet light
519 with a TiO_2 metasurface. *Nano Letters* **19**, 8972-8978 (2019).
520 8. Semmlinger, M. et al. Vacuum ultraviolet light-generating metasurface.
521 *Nano Letters* **18**, 5738-5743 (2018).
522 9. Shen, K. C. et al. Deep - ultraviolet hyperbolic metacavity laser.
523 *Advanced Materials* **30**, 1706918 (2018).
524 10. Kang, M. S. et al. Submicrometer-scale pattern generation via maskless
525 digital photolithography. *Optica* **7**, 1788-1795 (2020).
526 11. Liu, Y. H. et al. λ/12 super resolution achieved in maskless optical
527 projection nanolithography for efficient cross-scale patterning. *Nano*
528 *Letters* **21**, 3915-3921 (2021).

Accepted Manuscript

ACCEPTED ARTICLE PREVIEW

529 12. Liang, Z. X. et al. Two-photon absorption under few-photon irradiation
530 for optical nanoprinting. *Nature Communications* **16**, 2086 (2025).
531 13. Zheng, L. et al. UV-LED projection photolithography for high-resolution
532 functional photonic components. *Microsystems & Nanoengineering* **7**, 64
533 (2021).
534 14. Watanabe, Y. et al. Development of deep ultraviolet optical maskless
535 exposure tool for advanced lithography. *Journal of Micro/Nanopatterning*,
536 *Materials*, *and Metrology* **22**, 041403 (2023).
537 15. Owa, S. Review of optical direct-write technology for semiconductor
538 manufacturing. *Journal of Micro/Nanopatterning*, *Materials*, *and*
539 *Metrology* **22**, 041402 (2023).
540 16. Galiullin, A. A. et al. Cost-effective laboratory matrix projection micro-
541 lithography system. *Micromachines* **15**, 39 (2024).
542 17. Deng, M. J. et al. Maximizing energy utilization in DMD-based projection
543 lithography. *Optics Express* **30**, 4692-4705 (2022).
544 18. Chen, J. T. et al. Digital inverse patterning solutions for fabrication of
545 high-fidelity microstructures in spatial light modulator (SLM)-based
546 projection lithography. *Optics Express* **32**, 6800-6813 (2024).
547 19. Chen, J. T. et al. Deep learning-driven digital inverse lithography
548 technology for DMD-based maskless projection lithography. *Optics &*
549 *Laser Technology* **180**, 111578 (2025).
550 20. Chan, K. F. et al. High-resolution maskless lithography. *Journal of*
551 *Micro/Nanolithography*, *MEMS*, *and MOEMS* **2**, 331-339 (2003).
552 21. Yao, N. et al. Improving resolution of superlens lithography by phase-
553 shifting mask. *Optics Express* **19**, 15982-15989 (2011).
554 22. Stuerzebecher, L. et al. High-resolution proximity lithography for nano-
555 optical components. *Microelectronic Engineering* **132**, 120-134 (2015).
556 23. Gan, Z. F. et al. Spatial modulation of nanopattern dimensions by
557 combining interference lithography and grayscale-patterned secondary

Accepted Manuscript

ACCEPTED ARTICLE PREVIEW

558 exposure. *Light*: *Science & Applications* **11**, 89 (2022).

559 24. Pan, Y. H. & Ma, X. Informatics-based computational lithography for
560 phase-shifting mask optimization. *Optics Express* **30**, 21282-21294
561 (2022).

562 25. Lee, C. et al. Concurrent optimization of diffraction fields from binary
563 phase mask for three-dimensional nanopatterning. *ACS Photonics* **10**,
564 919-927 (2023).

565 26. Martinsson, H. et al. Current status of optical maskless lithography.
566 *Journal of Micro/Nanolithography*, *MEMS*, *and MOEMS* **4**, 011003
567 (2005).

568 27. Huang, H. Z. et al. Adaptive pixel-by-pixel modulated 3-D morphometry
569 based on digital micromirror device. *IEEE Transactions on*
570 *Instrumentation and Measurement* **73**, 5012010 (2024).

571 28. Liu, X. et al. Measurement of optical coherence structures of random
572 optical fields using generalized Arago spot experiment. *Opto-Electronic*
573 *Science* **2**, 220024 (2023).

574 29. Mendoza-Yero, O. et al. Encoding complex fields by using a phase-only
575 optical element. *Optics Letters* **39**, 1740-1743 (2014).

576 30. Goorden, S. A. et al. Superpixel-based spatial amplitude and phase
577 modulation using a digital micromirror device. *Optics Express* **22**, 17999-
578 18009 (2014).

579 31. Zhu, L. & Wang, J. Arbitrary manipulation of spatial amplitude and phase
580 using phase-only spatial light modulators. *Scientific Reports* **4**, 7441
581 (2014).

582 32. Sparrow, C. M. On spectroscopic resolving power. *Astrophysical Journal*
583 **44**, 76 (1916).

584 33. Masters, B. R. Abbe's theory of image formation in the microscope. in
585 Superresolution Optical Microscopy: the Quest for Enhanced Resolution
586 and Contrast. (ed Masters, B. R.) (Cham: Springer, 2020), 65-108.

Accepted Manuscript

587 34. Li, Y. L. et al. A further analysis of the forbidden pitch in
588 photolithography in advanced technology nodes. Proceedings of the
589 2023 IEEE 15th International Conference on ASIC. Nanjing: IEEE 2023:
590 1-4.
591 35. Apostol, Ş. & Hurley, P. Forbidden pitches: causes, source optimization,
592 and their role in design rules. Proceedings of SPIE 9426, Optical
593 Microlithography XXVIII. San Jose: SPIE, 2015, 404-413.
594 36. Liang, Z. X. et al. Diffraction-limit-breaking digital projection lithography
595 via multi-exposure strategies for high-density nanopatterning.
596 *Microsystems & Nanoengineering* **12**, 18 (2026).
597 37. Ronse, K. et al. Fundamental principles of phase shifting masks by
598 Fourier optics: theory and experimental verification. *Journal of Vacuum*
599 *Science & Technology B* **12**, 589-600 (1994).
600 38. Li, J. Q. et al. Nanoscale multi-beam lithography of photonic crystals
601 with ultrafast laser. *Light*: *Science & Applications* **12**, 164 (2023).
602 39. Hong, L. H. et al. Synergistic nonreciprocity of linear and nonlinear
603 optical diffraction. *Physical Review Letters* **133**, 223801 (2024).
604 40. Liu, J. H. et al. Fast wafer focus measurement system for
605 photolithography using on-axis structure illumination method. *Optics and*
606 *Lasers in Engineering* **162**, 107412 (2023).
607 41. Ding, H. W. et al. Off-axis illumination to solve the forbidden pitch
608 problem in plasmonic lithography. *Optics & Laser Technology* **183**,
609 112253 (2025).
610 42. Ma, X. et al. Optimization of lithography source illumination arrays using
611 diffraction subspaces. *Optics Express* **26**, 3738-3755 (2018).
612 43. Lin B J. Optical Lithography: Here is Why. 2nd edn. (Bellingham: SPIE,
613 2021).
614 44. Giannopoulos, I. et al. Extreme ultraviolet lithography reaches 5 nm
615 resolution. *Nanoscale* **16**, 15533-15543 (2024).

Accepted Manuscript

616 45. Han, D. D. et al. Quantitative analysis and modeling of line edge
617 roughness in near-field lithography: toward high pattern quality in
618 nanofabrication. *Nanophotonics* **8**, 879-888 (2019).
619 46. Zhao, Y. H. et al. LIC-CGAN: fast lithography latent images calculation
620 method for large-area masks using deep learning. *Optics Express* **32**,
621 40931-40944 (2024).
622 47. Li, Z. Q. et al. Decomposition-learning-based thick-mask model for
623 partially coherent lithography system. *Optics Express* **31**, 20321-20337
624 (2023).
625 48. Lanza, M. et al. The growing memristor industry. *Nature* **640**, 613-622
626 (2025).
627 49. Moon, J. H. et al. Materials quest for advanced interconnect
628 metallization in integrated circuits. *Advanced Science* **10**, 2207321
629 (2023).
630 50. Raza, A. et al. Advances, application and challenges of lithography
631 techniques. Proceedings of the 2024 5th International Conference on
632 Advancements in Computational Sciences. Lahore: IEEE, 2024, 1-6.

633

Accepted Manuscript